Analysis of the Lowest Order Cladding Mode of Long Period Fiber Gratings near Turn Around Point

Tanoy Kumar Dey, Sara Tombelli, Palas Biswas, Ambra Giannetti, Nandini Basumallick, Francesco Baldini, Somnath Bandyopadhyay, and Cosimo Trono

***Abstract*— A long period fiber grating (LPFG) sensor has been fabricated, after theoretical analysis, obtaining the maximum enhancement of the evanescent field working with the lowest order cladding mode ($LP_{0,2}$ cladding mode) near turn around point. Both the wavelengths of the dual peak resonance and the coupling conditions of the mode have been analyzed in detail. A flow cell has been fabricated to characterize the sensor in term of surrounding refractive index (SRI) sensitivity. The sensitivity of the sensor resulted to be ~ 8751 nm/SRIU, with a resolution in the order of 10^{-5}, within the SRI range of 1.333 to 1.3335.**

***Index Terms*—Long period fiber gratings, turn around point, evanescent field, etching.**

I. Introduction

LONG period fiber gratings (LPFGs) have been widely used throughout these years as biosensors and chemical sensors due to their ability to sense surrounding refractive index (SRI) variations [1-3]. In most of the bio-chemical sensing applications the surrounding medium is water or an aqueous buffer solution with a RI around 1.333 [4-6], where a conventional LPFG has low sensitivity [7]. For this purpose, it is necessary to enhance the sensitivity of LPFGs within this RI region. Different methodologies have been adopted to enhance the sensitivity, which can be classified in three main categories:

1) LPFGs operating near the mode transition region: in this case a thin layer of a material having a RI higher than the core medium is deposited on the fiber surface and its thickness is optimized (optimum overlay thickness) in order to have a significant increase of the SRI sensitivity [4,8,9-11].
2) LPFGs operating near the cladding modes (CMs) turn-around point (TAP): TAP can be obtained by controlling the period of the grating [12] or by varying the cladding diameter after grating inscription [13].
3) Enhancement of the CMs evanescent field: this can be obtained either by coupling light to higher order CMs [12] or by reducing the cladding diameter [14,15].

Combination of these three methodologies has also been observed [16-21]. As for the first strategy, obtaining mode transition requires different techniques of overlay deposition: some of them are very expensive and some require very complicated chemical post-processing after LPFG inscription [4, 19-21]. On the contrary, the other two methodologies are rather easy to implement by controlling the grating period during inscription and by reducing the cladding diameter by a chemical etching process [17]. For this reason, the last two sensitivity enhancement methodologies have been here considered in order to obtain highly sensitive LPFGs in aqueous medium.

Recently, it has been shown that by reducing the cladding diameter of a LPFG, a lower order CM (dispersed CM) can be obtained near TAP [17, 22]. The dispersed lower order CM becomes more sensitive than the normal higher order CM near TAP due to the enhancement of the evanescent field [17, 22]. However, until now, to the best of our knowledge, no detailed work has been reported on the enhancement of the LPFG evanescent field by attaining the lowest order dispersed CM near TAP.

In this work, we theoretically designed a LPFG on a 125 μm diameter fiber and then reduced the cladding diameter up to about 20 μm, until the TAP of $LP_{0,2}$ dispersed CM (lowest order CM) appeared. The position of the TAP of the $LP_{0,2}$ was optimized by controlling the grating period in such a way that the left peak of the dispersed mode appeared in C band (1525 nm - 1565 nm). We also showed that the variation of the transmission loss (TL) of $LP_{0,2}$ dispersed CM depends directly on the initial coupling condition (RI change induced during the grating inscription). Afterwards, we fabricated the optimized RI sensor and characterized it within a SRI range of 1.333 to 1.3335. The main problem with a so thin fiber is related to its fragility and difficult handling: for this reason, a closed flow

This paragraph of the first footnote will contain the date on which you submitted your paper for review. This work was supported by SERB, Government of India, for providing overseas visiting doctoral fellowship (ODF/2018/000288) to Tanoy Kumar Dey". *(Corresponding authors: Cosimo Trono, Somnath Bandyopadhyay).*

T. K. Dey, P. Biswas, N. Basumallick, S. Bandyopadhyay are with the Central Glass and Ceramic Research Institute, CSIR-CGCRI, 196 Raja S C Mullick Road, Kolkata 700032, India (email: tanoykumardey@gmail.com, palas@cgcri.res.in, nandini_b@cgcri.res.in, somnath@cgcri.res.in).

S. Tombelli, A. Giannetti, F. Baldini, C. Trono are with the Institute of Applied Physics "Nello Carrara", CNR-IFAC, Via Madonna del Piano 10, 50019 Sesto Fiorentino, Italy (email: s.tombelli@ifac.cnr.it, a.giannetti@ifac.cnr.it, f.baldini@ifac.cnr.it, c.trono@ifac.cnr.it).

cell was designed and fabricated, for the sensitivity characterization. With this optimized design, the sensitivity of the sensor resulted to be 8751 nm/SRIU with a resolution in the order of 10^{-5}.

II. Design and Simulation

In LPFGs, the fundamental core mode ($LP_{0,1}$ mode) couples with different higher order co-propagating CMs ($LP_{0,m}$ mode with m=2,3,4….) at the wavelength where the following resonance condition is satisfied:

$$\lambda_{res} = (n_{eff}^{co} - n_{eff}^{cl\ 0,m})\Lambda \quad (1)$$

where n_{eff}^{co} and $n_{eff}^{cl\ 0,m}$ are the effective refractive index of the fundamental core mode and of the m[th] order CM, respectively, and Λ is the period of the grating [12].

It is known that when a CM is approaching the TAP, a dual resonance is obtained [12], which is highly sensitive to SRI, reaching the maximum sensitivity exactly at TAP, with a single broadband attenuation in the transmission spectrum. As the order of the CM increases by reducing the grating period for a non-etched fiber, the SRI sensitivity near TAP also increases. However, recently it has been shown that, alternatively to operating on the grating period, if the cladding diameter is reduced the resonance wavelength of the left peak shifts towards the red region up to the TAP position, and the evanescent field of the lower order dispersed CM, and consequently, its sensitivity, increases more than the one of the higher order mode of the non-etched fiber [17,22].

In this section we report the numerical characterization of the lowest order dispersed CM ($LP_{0,2}$) near TAP, obtained by the highest possible cladding diameter reduction, to get the maximum enhancement of the evanescent field and of the sensitivity working in the C band. Subsequently, the optimization of the position of the $LP_{0,2}$ dispersed CM near TAP is accomplished by tuning the period of the grating, and by optimizing the coupling condition as a function of the amount of induced RI modulation. The fiber and grating parameters chosen for our simulation (by Optigrating 4.2) are reported in Table 1. The spectrum calculated with these parameters is shown in Fig. 1.

TABLE I
Fiber and Grating Parameters

Name of the parameters	Values used for simulation
Core RI	1.44985
Cladding RI	1.44400
Core diameter	7.3 µm
Fiber diameter	124.6 µm
Index modulation (Δn)	8×10^{-5}
Grating period (Λ)	246 µm
No. of grating planes	123
Grating length	30.012 mm

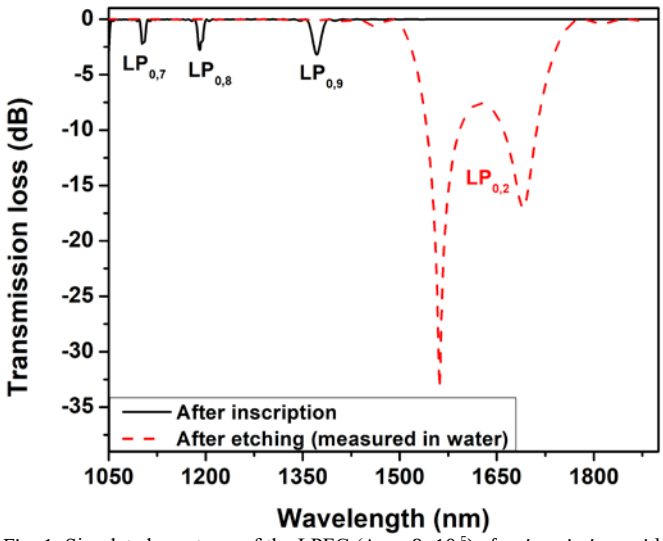

Fig. 1. Simulated spectrum of the LPFG ($\Delta n = 8\times10^{-5}$) after inscription, with $LP_{0,9}$ mode in under-coupled condition (black line); spectrum of the maximum coupled $LP_{0,2}$ dispersed CM near TAP after etching (red dashed line).

The $LP_{0,9}$ mode has been generated at 1370 nm and the corresponding TL of this mode is – 3.2 dB (Fig. 1, black line). Then the cladding diameter is reduced up to 20.284 µm so that the TAP of $LP_{0,2}$ dispersed CM appears in water medium (RI 1.333), with dual peak separation of ~ 130 nm, as shown in Fig. 1 (red line). The 130 nm peak to peak separation has been chosen to have a sufficient resolution between the two peaks. This is the maximum possible etching for the LPFG as $LP_{0,2}$ is the lowest order CM. Beyond this diameter, the resonant condition of the LPFG is no more satisfied.

It is clear from Fig. 1 that $LP_{0,9}$ mode and, as a consequence, all the lower CMs are under-coupled before etching ($kL<\pi/2$; k= coupling coefficient of a CM and L= length of the grating), because of the low value of Δn (it is known that, for a given fiber diameter and grating length, the coupling coefficient increases with increment of the mode number [12]). Conversely, after etching, the $LP_{0,2}$ dispersed CM attains the maximum coupling condition ($kL\sim\pi/2$), because the reduction of the cladding diameter directly influences the coupling coefficient of the CMs. To verify this hypothesis, we changed the index modulation Δn from 8×10^{-5} to 2×10^{-4} to attain the maximum coupling condition of the $LP_{0,9}$ mode (Fig. 2). When the cladding diameter is reduced to obtain the TAP of the $LP_{0,2}$ dispersed CM in water medium, the $LP_{0,2}$ coupling coefficient enhances to such a value that this mode becomes over-coupled ($kL>\pi/2$) as shown in Fig. 2. At this point, it is important to observe that the optimum value of Δn must be chosen, in order to achieve the maximum coupling condition (and consequently the maximum TL) for the $LP_{0,2}$ dispersed CM near TAP, because, in real experiments, higher TL gives rise to more precise determination of the resonance wavelength, reducing the standard deviation and so improving the limit of detection (LOD).

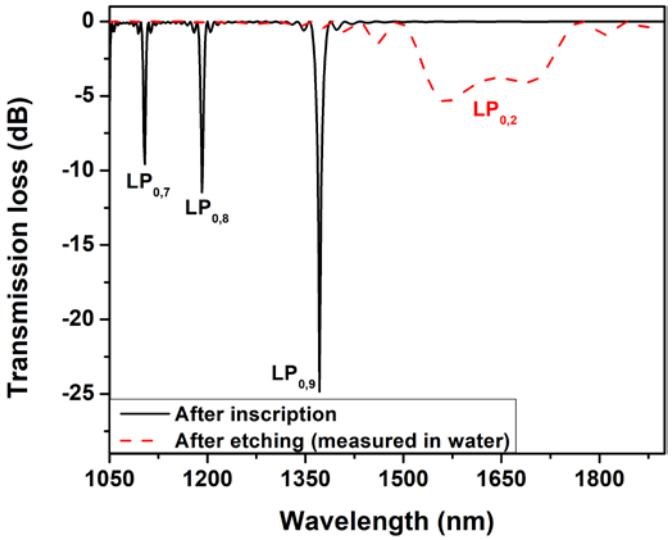

Fig. 2. Simulated spectrum of the LPFG ($\Delta n = 2\times10^{-4}$) after inscription, with $LP_{0,9}$ mode in maximum coupling condition (black line); spectrum of over coupled $LP_{0,2}$ dispersed CM near TAP after etching (red dashed line).

The choice of the grating period is also very important as this is directly related with the position of the $LP_{0,2}$ dispersed CM near TAP. The spectra of this mode near TAP in water medium with grating periods Λ = 236 µm, 246 µm and 256 µm are shown in Fig. 3. In all cases, Δn is considered to be 8×10^{-5} and the separation of the dual peak is maintained at ~ 130 nm. It is clear from Fig. 3 that the spectrum shifts towards the shorter wavelength direction as the grating period is decreasing. We targeted to place the left peak of the $LP_{0,2}$ dispersed CM at ~1560 nm, so that during the SRI sensitivity measurement the whole wavelength shift of the left peak would remain in the C band.

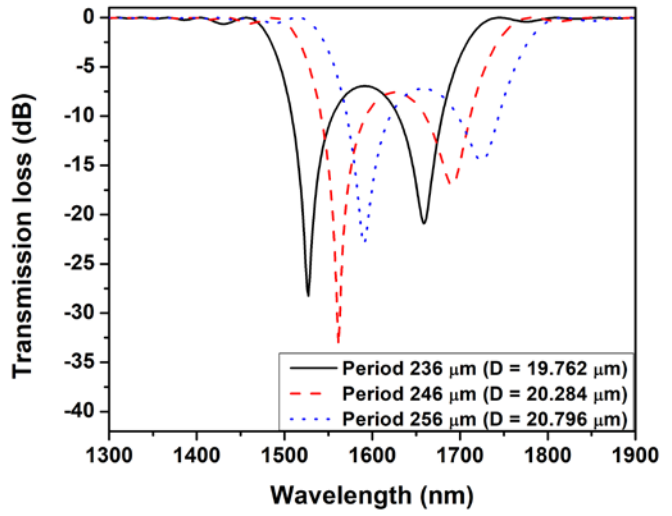

Fig. 3. Simulated spectra of $LP_{0,2}$ dispersed CM near TAP, with different grating period, in SRI 1.333.

To be noted that, when decreasing the period, the cladding diameter needs to be slightly reduced to maintain the equal dual peak separation: for the 236 µm period the fiber diameter is considered to be 19.762 µm whereas for the 256 µm one the diameter is 20.796 µm. Moreover, by controlling the period of the grating, the right peak of the $LP_{0,2}$ dispersed CM can be generated within C band: to this aim, the cladding diameter needs to be further reduced.

Theoretically, all the higher order modes should have more sensitivity than the $LP_{0,2}$ CM near TAP. However, in the operating conditions proper of the work here reported, keeping the fiber diameter around 20 µm and tailoring the period to excite the $LP_{0,3}$ mode in the available bandwidth, we found out that the TAP is far away (blue direction) from the bandwidth. Only the right peak of the $LP_{0,3}$ mode could be observed within the available bandwidth and the same occurred for all the other CMs higher than $LP_{0,2}$ (data not shown). Consequently, for these modes the optimum sensitivity could not be obtained.

III. Experimental Results and Discussion

A. *LPFG fabrication*

The LPFG was fabricated by using the point-by-point inscription technique with a KrF excimer laser (Lambda Physics Compex 110) on Fibercore PS1250/1500 B/Ge co-doped photosensitive fibers. The period of the LPFG was Λ=246 µm and the number of grating planes was 123, with a resulting calculated grating length of 30.012 mm. The laser beam was shaped by means of a micrometric slit (123 µm aperture, 50% duty cycle), and was focused along the axis of the fiber by using a cylindrical lens after stripping 40 mm of the polymeric jacket of the fiber. The position of the LPFG was kept at the middle portion of the stripping region. The total pulses per grating plane are 80 and the total fluence was 22.4 J/cm^2. The resulting LPFG spectrum is shown in Fig. 4. The $LP_{0,9}$ mode at ~1370 nm and the corresponding TL of –5 dB, well match with the simulation result. All the spectra were measured using a SLED source (FiberLabs Inc. SLD-1310/1430/1550/1690-10) and an optical spectrum analyzer (OSA; Anritsu MS9030A/9701C). The minimum wavelengths were calculated by fitting the resonant band with a Lorentzian function. The bandwidth was considered from 1300 nm to 1700 nm depending on the SLED source band and on the cut-off wavelength of the used fiber (1209 nm). As a result, at the moment of fabrication, it was not possible to detect CMs of orders lower than $LP_{0,9}$, because the resonant wavelengths of those modes are below 1250 nm as shown in the simulation result (Fig. 1).

B. *Etching procedure*

The fiber was dipped in a 20% hydrofluoric acid (HF) solution for chemical etching. During this process, keeping the fiber straight was of fundamental importance in order to avoid bending induced perturbations caused by the reduced fiber diameter (~ 20 µm, according to the calculation). In addition, special care was given to the handling of this low diameter fiber as any unwanted mechanical strength along the longitudinal or transverse direction can cause its breakage. Therefore, before starting the etching process the fiber was clamped to a suitable u-shaped support by means of two magnetic holders (Fig. 5) and throughout the etching process the fiber was not touched. The LPFG was kept at the center of the u-shaped support.

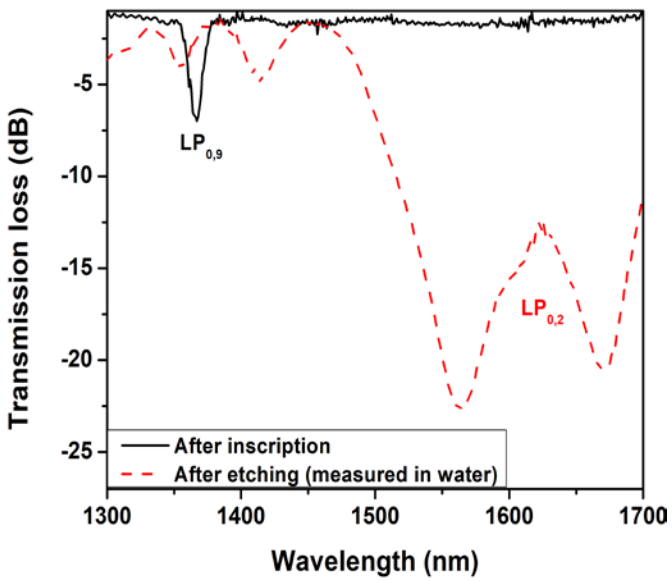

Fig. 4. Measured spectra of the fabricated LPFG after inscription (black line) and after cladding diameter reduction (red dashed line).

Etching was done until (~ 4 h) the TAP of the $LP_{0,2}$ dispersed CM appeared in the water medium (RI 1.333) as shown in Fig. 4.

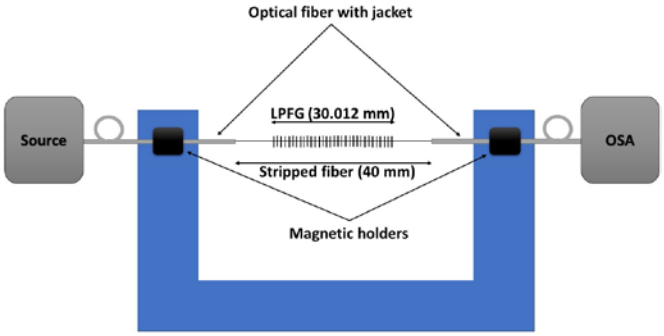

Fig. 5. Schematic of the u-shaped support of the optical fiber during the etching process.

A microscopic image of the etched fiber is shown in Fig. 6. The measured diameter of the etched fiber was found out to be 21.87 µm (20× magnification), which was well matched with the previous calculations.

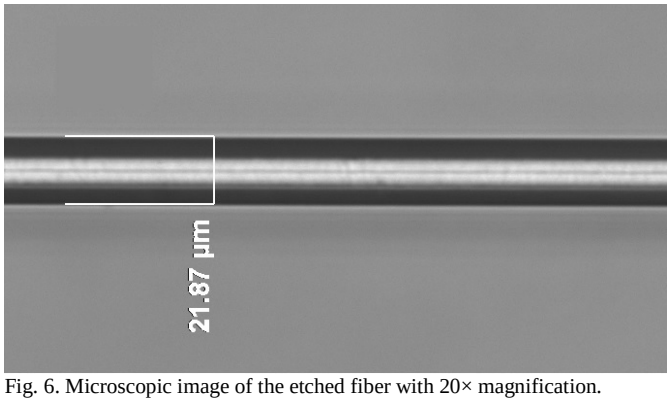

Fig. 6. Microscopic image of the etched fiber with 20× magnification.

The spectral evolution of the left peak of the $LP_{0,7}$ dispersed CM (taken as an example) is shown in Fig. 7A and the minimum of each spectrum (TL) at its corresponding resonant wavelength is shown in Fig. 7B. The left peak moved towards the red direction as a function of the etching process, and it disappeared after merging with the right peak at the TAP. During evolution of the spectrum of $LP_{0,7}$ CM only the left peak was observed within the wavelength range 1300 nm to 1700 nm as TAP of the corresponding mode was beyond 1700 nm.

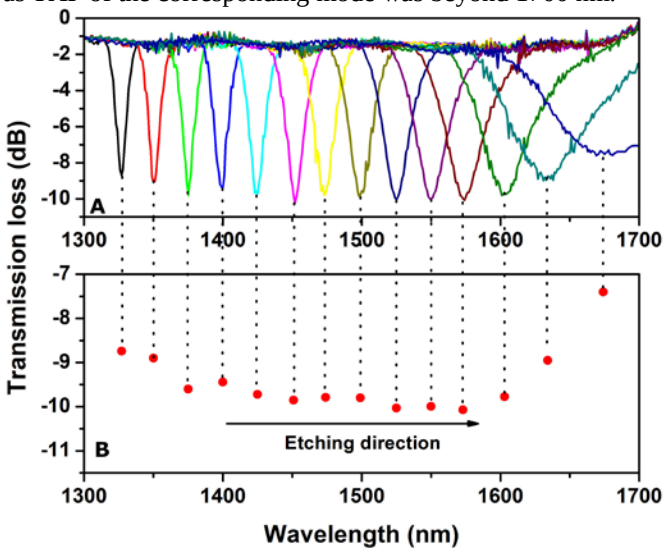

Fig. 7. A) Spectral evolution of the $LP_{0,7}$ CM during the etching process. B) Minima of each spectra at their corresponding resonant wavelength.

The variation of the left peak TL (proportional to the coupling coefficient) of $LP_{0,9}$, $LP_{0,7}$, $LP_{0,5}$ and $LP_{0,2}$ CMs (other modes have the same trends but are not shown for simplifying the graph) during the etching process is shown in Fig. 8 by using the same plotting approach of Fig. 7. From $LP_{0,9}$ to $LP_{0,2}$ the enhancement of TL was clearly observed at every wavelength; in addition, as the spectrum was moving in the red direction, the TL of each mode gets reduced while approaching TAP (see also Fig. 7A), except for $LP_{0,9}$, as the TAP of this CM was far away from 1700 nm. The TAP of dispersed CMs shifted toward shorter wavelengths as a function of the etching diameter, and the etching process was stopped when the $LP_{0,2}$ left peak was at ~1560 nm and the dual peak separation was 104 nm.

It is clear from Fig. 8 that the $LP_{0,2}$ mode is in the best coupling condition with TL> -20 dB near TAP in water medium. The sensor optimization process was concluded at this stage, having reduced the cladding diameter to its maximum possible value, with the period Λ and the RI modulation Δn optimized in such a way that the $LP_{0,2}$ dispersed CM attains the best coupling condition ($kL \sim \pi/2$) near TAP in water medium with its left peak in the C band.

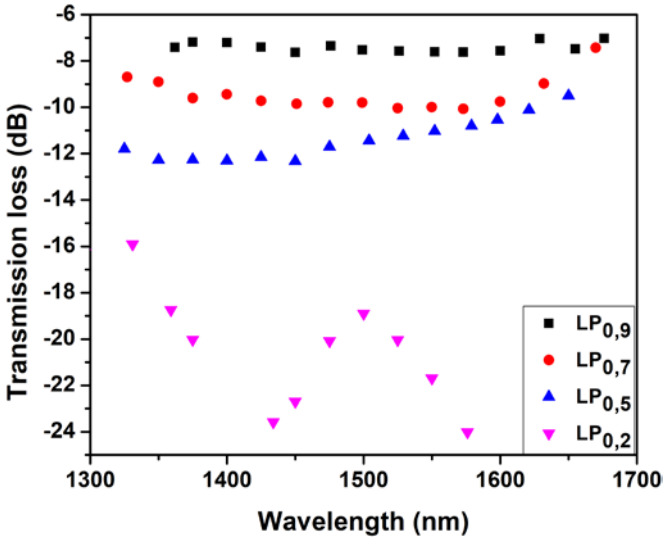

Fig. 8. Variation of the transmission loss of the left peak of different CMs during the etching process.

C. *RI sensitivity analysis*

For the sensitivity analysis, 0.0% - 0.5% w/v sodium chloride (NaCl) water solutions (RI in the range 1.333 to 1.3335 [23]) was used. At first a poly(methyl methacrylate) (PMMA) open cell fixed on a lab jack (Newport 281) was used to contain the solutions and the LPFG was dipped into the solutions by lifting the cell up. To keep the fiber straight and to avoid its damage, the LPFG was not removed from the u-shaped support used during the etching process. In this configuration, the influence of the surrounding temperature and the perturbations induced when the fiber was kept in air during the exchange of the solutions in the cell, strongly affected the wavelength shift measurements in the different RI solutions. In addition, the fragility and the difficulty of handling a so thin fiber hampered the measurement of the sensitivity in the open cell.

To remove these limitations and protect the fiber, we designed a PMMA closed flow cell. This cell was composed by two parts: the lower part is constituted by a PMMA slide (79 mm ×27 mm × 1.5 mm), whereas the upper part, shown in Fig. 9, was made by using a 76 mm×26 mm×5 mm PMMA block. A flow channel, 50 mm long and 1.5 mm deep, was created along the center of the block. To avoid the damage of the fiber, the length of this portion was greater than the etched region (40 mm). V grooves, where the jacketed part of the fiber had to be fixed, were created at the two ends of the flow channel. Two holes (1.5 mm in diameter), drilled from the top in correspondence of the ends of the flow channel, were used as fluidic inlet and outlet (Fig. 9B). Two slots of dimension 76 mm × 6 mm × 1 mm, were created on both the sides of the channel, and a hole, 1.5 mm in diameter and 23 mm in length, was created on the lateral side to place a thermocouple for temperature monitoring, as shown in Fig. 9A.

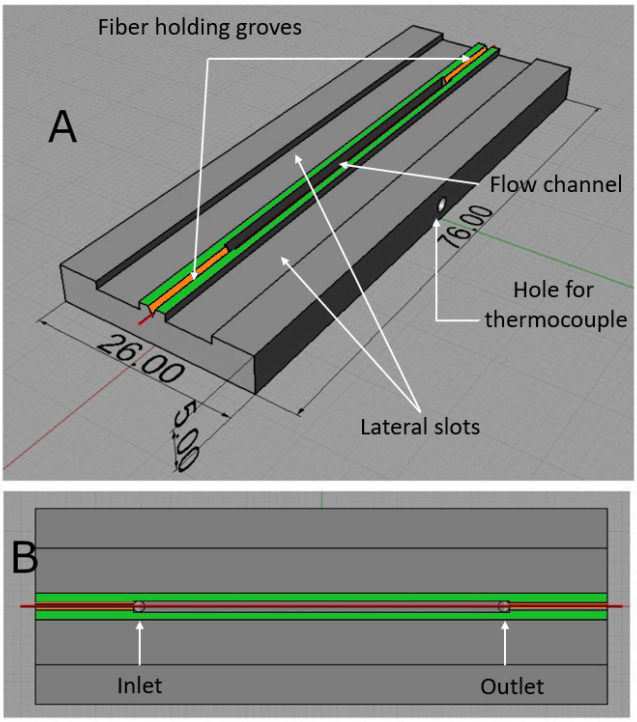

Fig. 9. Scheme of the upper part of the closed flow cell; A) 3D view (measurements are given in mm), B) Top view. The red line indicates the fiber, the two green strips are the lateral borders of the flow channel and the orange strips defines the V-grooves where the fiber is glued.

The fiber fixing procedure is the following: firstly, the top part of the cell was positioned under the etched fiber (kept straight by the u-shaped support) in such a way that the etched region was centered in the flow channel, and the jacketed region was fixed in the V groves by means of Norland NOA60 UV-curing optical adhesive. Then, the bottom part was used to seal the channel by putting the optical adhesive on the narrow lateral strips which delimit the flow channel (indicated in green color in Fig. 9). The aim of the two 6 mm wide and 1 mm deep lateral slots was to reduce the surface used to glue the top and bottom part. In this way, the overflowing of the adhesive inside the flow channel after placing the bottom part was avoided. Two stainless steel tubes of length 15 mm and diameter 1.5 mm were fixed inside the holes for the connection to a peristaltic pump (MINIPLUS 3). A photo of the complete flow cell is depicted in Fig. 10.

Once sealed into the flow cell, LPFG was prevented from bending loss and its handling was easier, because the portion of the fiber coming out from the two ends of the cell was jacketed. The measurement protocol is the following:

1) pulling of the solution inside the flow cell at a flow rate of ~ 85 uL/min for 5 minutes;
2) stop flow with the acquisition of the resonance wavelength for 3 minutes (8 measured spectra).

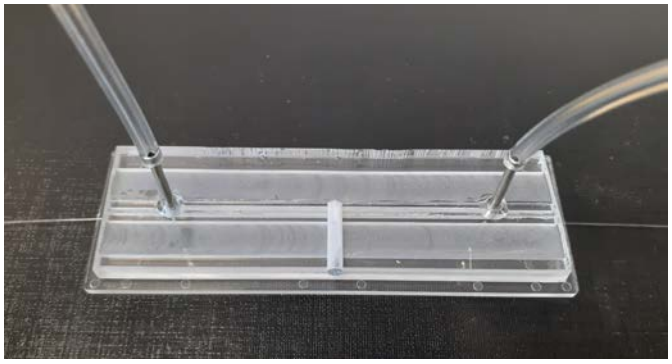

Fig. 10. Photo of the closed flow cell with the fluidic connections.

All the solutions were pulled in the flow channel without bringing the fiber in contact with air. The sensorgram (wavelength shift vs time) of the right peak of the $LP_{0,2}$ dispersed CM is shown in Fig. 11 where the shaded region is indicating the stop flow condition (pump off) and the non-shaded region is indicating the flowing condition (pump on). The flow rate and the flow time were chosen in order to ensure the complete exchange of the different solutions inside the channel.

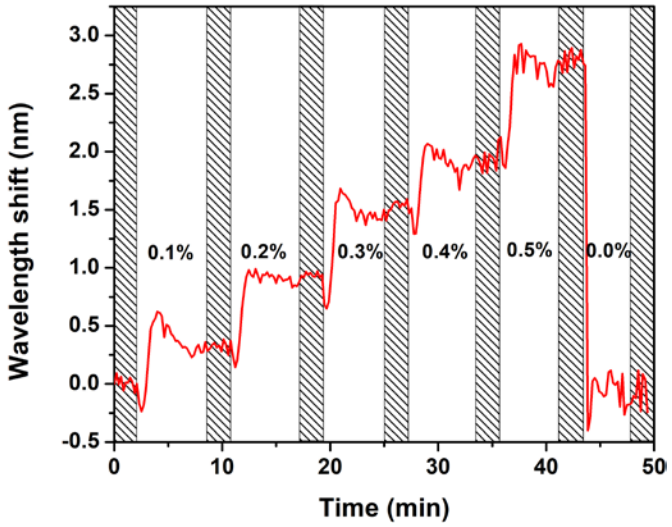

Fig. 11. Sensogram (wavelength shift vs time) of the right peak of the $LP_{0,2}$ dispersed CM during the sensitivity analysis in the closed flow cell.

The resonant wavelength and the error for each tested RI are calculated as the average and the standard deviation of the 8 measurements (resonance wavelength calculated through the Lorentzian fit) acquired during the stop flow phase (3 minutes). The wavelength shift as a function of surrounding RI is depicted in Fig. 12, considering the wavelength at RI 1.333 as reference point. The sensitivity of the left, right and dual peak, calculated as the slope of the linear regression lines, are 3342 nm/SRIU, 5409 nm/SRIU and 8751 nm/SRIU respectively (Fig. 12).

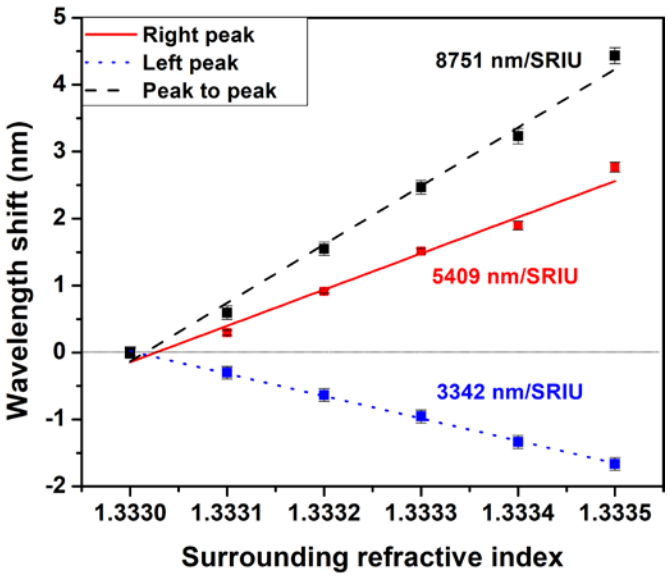

Fig. 12. Sensitivity analysis of the $LP_{0,2}$ dispersed CM near TAP.

The resonant wavelength of the $LP_{0,2}$ dispersed CM measured in water (0% NaCl) at the end of the sensitivity characterization (Fig. 11, from min 44 to min 50), returned back to the initial value, demonstrating the absence of hysteresis in the measurement system. The resolution, calculated as three times the average standard deviation, is 5×10^{-5} RIU. In [17] a SRI sensitivity of nearly the same order has been achieved with the $LP_{0,3}$ CM. However, in that case, an optical fiber of different dimension has been used and the SRI characterisation is performed in the RI range 1.353-1.398, where the LPFG sensitivity is usually greater, whereas, for biosensing application, the sensor needs to attain its maximum sensitivity at ~ 1.333 SRI.

IV. Conclusion

An etched LPFG sensor near TAP at the lowest order dispersed CM ($LP_{0,2}$), where the evanescent field was the highest, was designed and fabricated. The spectral position of the dispersed CM was controlled in term of the grating period and the coupling condition was tuned by tailoring the RI modulation of the grating. The sensor was characterized in term of SRI sensitivity. In order to ensure a better handling of the etched fiber and to avoid external perturbations, an ad hoc closed flow cell was designed and fabricated for the experimental evaluation of the sensitivity of the LPFG sensor. The obtained SRI dual peak sensitivity is 8751 nm/RIU, with a resolution of 5×10^{-5} RIU. Despite its low mechanical strength, this sensor, with a proper packaging within the flow cell, can be considered very promising for bio-chemical sensing applications.

Acknowledgement

The authors would like to thank SERB, Government of India, for providing overseas visiting doctoral fellowship (ODF/2018/000288) to Tanoy Kumar Dey.

REFERENCES

[1] F. Chiavaioli, F. Baldini, S. Tombelli, C. Trono, A. Giannetti, "Biosensing with optical fiber gratings," *Nanophotonics*, vol. 6, no. 4, pp. 663-679, Jun. 2017.

[2] S. Korposh, S. Lee, S. James, "Long Period Grating Based Fibre Optic Chemical Sensors," in *Fiber optic sensors current status and future possibilities*, Smart Sensors, Measurement and Instrumentation book series, vol. 21, Springer, 2017, pp. 241–267.

[3] S. W. James, R. P. Tatam, "Optical fiber long-period grating sensors: Characteristics and application," *Meas. Sci. Technol.*, vol. 14, pp. R49-R61, Mar. 2003.

[4] F. Yang, T. Chang, T. Liu, D. Wu, H. Du, J. Liang, F. Tian, "Label- free detection of Staphylococcus aureus bacteria using long-period fiber grating with functional polyelectrolyte coatings," *Biosens. Bioelectron.*, vol. 133, pp. 147-153, May. 2019.

[5] F. Esposito, L. Sansone, C. Taddei, S. Campopiano, M. Giordano, A. Iadicicco, "Ultrasensitive biosensor based on long period grating coated with polycarbonate-graphene oxide multilayer," *Sens. Actuators B Chem.*, vol. 274, pp. 517-526, Nov. 2018.

[6] M. Janczuk-Richter, M. Piestrzynska, D. Burnat, P. Sezemsky, V. Stranak, W. J. Bock, R. Bogdanowicz, J. Niedziolka-Jonsson, M. Smietana, "Optical investigation of electrochemical process using a long-period fiber grating functionalized by indium tin oxide," Sens. Actuators B Chem., vol. 279, pp. 223-229, Jan. 2019.

[7] H. J. Patrick, A. D. Kersey, F. Bucholtz, "Analysis of the response of long period fiber grating to external index of refraction," *J. Lightwave Technol.*, vol. 16, no. 9, pp. 1606–1612, Sep. 1998.

[8] I. D. Villar, I. R. Matias, F. J. Arregui, P. Lalanne, "Optimization of sensitivity in long period fiber grating with overlay deposition," *Opt. Express*, vol. 13, no. 1, pp. 56–69, Jan. 2005.

[9] F. Chiavaioli, P. Biswas, C. Trono, S. Jana, S. Bandyopadhyay, N. Basumallick, A. Giannetti, S. Tombelli, S. Bera, A. Mallick, F. Baldini, "Sol-gel-based titania-silica thin film overlay for long period fiber grating based biosensors," *Anal. Chem.*, vol. 87, no. 24, pp. 12024–12031, Nov. 2015.

[10] P. Pilla, P. Foglia Manzillo, V. Malachovska, A. Buosciolo, S. Campopiano, A. Cutolo, L. Ambrosio, M. Giordano, A. Cusano, "Long period grating working in transition mode as promising technological platform for label free biosensing," *Opt. Exp.*, vol. 17, no. 22, pp. 20039-20050, Oct. 2009.

[11] P. Pilla, V. Malachovska, A. Borriello, A. Buosciolo, M. Giordano, L. Ambrosio, A. Cutolo, A. Cusano, "Transition mode long period grating biosensor with functional multilayer coatings," *Opt. Exp.*, vol. 19, no. 2, pp. 512-526, Jan. 2011.

[12] X. Shu, L. Zhang, I. Bennion, "Sensitivity characteristics of long-period fiber grating," *J. Lightwave Technol.*, vol. 20, no. 2, pp. 255–266, Feb. 2002.

[13] P. Biswas, N. Bsumallick, S. Bandyopadhyay, K. Dasgupta, A. Ghosh, S. Bandyopadhyay, "Sensitivity enhancement of turn-around-point long period grating by tuning initial coupling condition," *IEEE Sens. J.*, vol. 15, no. 2, pp. 1240–1245, Feb. 2015.

[14] K. S. Chiang, Y. Liu, M. N. Ng, and X. Dong, "Analysis of etched long-period fiber grating and its response to external refractive index," *Electron. Lett.*, vol. 36, no. 11, pp. 966–967, May. 2000.

[15] M. Śmietana, M. Koba, P. Mikulic, W. J. Bock, "Measurements of reactive ion etching process effect using long-period fiber gratings," *Opt. Exp.*, vol. 22, no. 5, pp. 5986–5994, Feb. 2014.

[16] F. Zou, Y. Liu, C. Mou, S. Zhu "Optimization of refractive index sensitivity in nano-film coated long-period fiber grating near dispersion turning point," *J. Lightwave Technol.* DOI: 10.1109/JLT.2019.2949373, Oct. 2019.

[17] I. D. Villar, J. L. Cruz, A. B. Socorro, J. M. Corres, I. R. Matias, "Sensitivity optimization with cladding-etched long period fiber gratings at dispersion turning point," *Opt. Exp.*, vol. 24, no. 16, pp. 17680–17685, Aug. 2016.

[18] I. D. Villar, "Ultrahigh-sensitivity sensors based on thin-film coated long period grating with reduced diameter, in transition mode and near the dispersion turning point," *Opt. Exp.*, vol. 23, no. 7, pp. 8389–8398, Mar. 2015.

[19] M. Piestrzyńska, M. Dominik, K. Kosiel, M. Janczuk-Richter, K. Szot-Karpińska, E. Brzozowska, L. Shao, J. Niedziółka-Jonsson, W. J. Bock, M. Śmietana, "Ultrasensitive tantalum oxide nano-coated long-period grating for detection of various biological targets," *Biosens. Bioelectron.*, vol. 133, pp. 8-15, Mar. 2019.

[20] M. Śmietana, M. Koba, P. Mikulic, W. J. Bock, "Towards refractive index sensitivity of long period gratings at level of tens of μm per refractive index unit: fiber cladding etching and nano-coating deposition," *Opt. Exp.*, vol. 24, no. 11, pp. 11897–11904, May. 2016.

[21] M. Smietana, M. Koba, P. Mikulic, W. J. Bock, "Combined plasma-based fiber etching and diamond-like carbon nanooverlay deposition for enhancing sensitivity of long-period grating," *J. Lightwave Technol.*, vol. 34, no. 19, pp. 4615–4619, Oct. 2016.

[22] T. K. Dey, P. Biswas, S. Bandyopadhyay, N. Basumallick, K. Dasgupta S. Bandyopadhyay, "Sensitivity analysis of a dispersed clad mode to surrounding refractive index", Presented at ICMAP 2015, DOI: 10.1109/ICMAP.2015.7408709., Dec. 2015.

[23] E. A. Barbosa, D. M. Silva, A. O. Preto, R. Verzini, "Design, construction, and performance of a real-time holographic refractometry prototype for liquid analysis," *Rev. Sci. Instrum.*, vol. 82, no. 19, pp. 013103 1-7, Jan. 2011.